


Ultralow-Power Orbital-Controlled Magnetization Switching Using a Ferromagnetic Oxide Interface

Le Duc Anh,^{1,2,*} Takashi Yamashita,¹ Hiroki Yamasaki,¹ Daisei Araki,¹ Munetoshi Seki,^{1,3}
Hitoshi Tabata,^{1,3} Masaaki Tanaka,^{1,3,†} and Shinobu Ohya^{1,2,3,‡}

¹*Department of Electrical Engineering and Information Systems, The University of Tokyo, 7-3-1 Hongo, Bunkyo-ku, Tokyo 113-8656, Japan*

²*Institute of Engineering Innovation, Graduate School of Engineering, The University of Tokyo, 7-3-1 Hongo, Bunkyo-ku, Tokyo 113-8656, Japan*

³*Center for Spintronics Research Network (CSRN), The University of Tokyo, 7-3-1 Hongo, Bunkyo-ku, Tokyo 113-8656, Japan*

 (Received 5 April 2019; revised manuscript received 23 August 2019; published 2 October 2019)

A major challenge in spin-based electronics is reducing power consumption for magnetization switching of ferromagnets, which is implemented by injecting a large spin-polarized current. The alternative approach is to control the magnetic anisotropy (MA) of the ferromagnet by an electric field. However, the voltage-induced MA is too weak to deterministically switch the magnetization without an assisting magnetic field and a strategy towards this goal remains elusive. Here, we demonstrate a scheme of orbital-controlled magnetization switching (OCMS). A sharp change in the MA is induced when the Fermi level is moved between energy bands with different orbital symmetries. Using a ferromagnetic oxide interface, we show that OCMS can be used to achieve a deterministic and magnetic-field-free 90°-magnetization switching solely by applying a small electric field of 0.05 V nm⁻¹ with a negligibly small current density of about 10⁻² A cm⁻². Our results highlight the huge potential of band engineering in ferromagnetic materials for efficient magnetization control.

DOI: [10.1103/PhysRevApplied.12.041001](https://doi.org/10.1103/PhysRevApplied.12.041001)

In present spin-based electronic devices, such as magnetic tunnel junctions (MTJs), magnetization switching is implemented by either spin transfer torque (STT) [1–3] or spin-orbit torque (SOT) [4,5]. These current-driven switching methods require a very large current density, typically in the order of 10⁶–10⁷ A cm⁻² for STT and 10⁵–10⁶ A cm⁻² for SOT, which causes high-power consumption, and thus, degrades the endurance and scalability of the device. Therefore, there is intensified interest in electric-field-driven schemes for magnetization switching, the key ingredient of which is to manipulate the magnetic anisotropy (MA) of ferromagnetic thin films using a bias voltage [6–16]. However, in ferromagnetic metals [11–14], the electron charging effect by an electric field is effective only in monolayer thin films, and modification is, at most, 10% of the total interfacial MA energy for a typical electric field of 1 V nm⁻¹, as also expected from density functional theory modeling [17]. Because of this small change in the MA energy, the demonstration

of electric-field-driven magnetization switching always requires an external magnetic field or a well-calibrated sequence of ultrafast electrical pulses [13], both of which are impractical for device applications. The magnetoelectric effect in multiferroic materials, such as BiFeO₃, is promising for reducing the power consumption of magnetization switching by an order of magnitude [15]; however, in these cases, the choice of materials is limited and very low device endurance is a problem.

In this Letter, we report that highly effective magnetization switching can be implemented by moving the Fermi level (E_F) between energy bands with different-symmetry orbitals, which is induced by a strong change of the MA through spin-orbit interactions [Fig. 1(a)]. We call this scheme orbital-controlled magnetization switching (OCMS). Using an MTJ composed of La_{0.67}Sr_{0.33}MnO₃ (LSMO)/SrTiO₃ (STO)/LSMO as a model system, we demonstrate a deterministic magnetic-field-free sharp 90° switching of magnetization induced solely by a small change in the electric field applied on the tunnel barrier (~0.05 V nm⁻¹), which is two orders of magnitude smaller than that of values reported in previous works, [11–14,17] with a negligibly small current density (~10⁻² A cm⁻²). These results also suggest that OCMS can possibly be

*anh@cryst.t.u-tokyo.ac.jp

†masaaki@ee.t.u-tokyo.ac.jp

‡ohya@cryst.t.u-tokyo.ac.jp

applied to a wide range of materials that have only moderate spin-orbit interactions, such as LSMO, if the band structure is appropriately designed.

To demonstrate OCMS, LSMO [18–20] is an ideal ferromagnetic material, thanks to its band structure. Immediately (~ 0.2 eV) below the E_F in LSMO, at the LSMO/STO interface, there is the bottom band edge of spin-up e_g orbitals and the top band edge of the t_{2g} orbitals [21,22]. We study a MTJ structure consisting of, from the top surface, LSMO [18 unit cells (u.c.) = 7.0 nm]/STO (10 u.c. = 3.9 nm)/LSMO (40 u.c. = 15.6 nm), which is etched into a circular mesa with a diameter of 800 μm [see Fig. 1(b) and the Supplemental Material [23]]. Our proposed scheme is illustrated in Fig. 1(c): when applying a positive bias voltage, V , for example, carrier depletion occurs at the top interface between LSMO and STO (left-side interface), which moves the chemical potential (μ) downward from the e_g band to the t_{2g} band and induces a sharp change in the MA of the top LSMO layer. To detect this change in the MA when changing V , we measure the characteristics of tunneling magnetoresistance (TMR) with a magnetic field, \mathbf{H} , applied along various in-plane directions (Fig. 2). Here, the TMR ratio is defined as $[R(\mathbf{H}) - R(0)]/R(\mathbf{H})$, in which $R(\mathbf{H})$ represents the tunnel resistance under \mathbf{H} ; $\theta_{\mathbf{H}}$, $\theta_{\mathbf{M}_t}$, and $\theta_{\mathbf{M}_b}$ are the in-plane angles of \mathbf{H} ; and \mathbf{M}_t is the magnetization vector of the top LSMO layer and \mathbf{M}_b is that of the bottom LSMO layer, from the [100] axis in the counterclockwise direction, as shown in Fig. 1(b). All crystallographic axes in this work

are defined with respect to the pseudocubic crystal structure of STO. In Figs. 2(a) and 2(b), at small V (15 mV), large and clear TMR switching occurs when \mathbf{H} is along the $[\bar{1}10]$ axis, while it is suppressed when \mathbf{H} is along the [110] axis. However, as $|V|$ is increased, the magnitudes of TMR ratios measured with $\mathbf{H}//[110]$ and $\mathbf{H}//[\bar{1}10]$ become nearly identical ($\sim 15\%$). This anomalous feature can be more clearly understood by comparing the V dependences of TMR between those \mathbf{H} directions in Fig. 2(c). The color-coded polar plots of $\text{TMR}(H, \theta_{\mathbf{H}})$ in Fig. 2(d) reveal a sharp transition from a dominantly twofold symmetry, with an easy axis lying along the $[\bar{1}10]$ direction (see the red regions), to an almost fourfold symmetry along the $\langle 110 \rangle$ axes with increasing V (see the emerging yellow regions along the [110] axis). This result means that the MA of the top LSMO layer does indeed change from two- to fourfold with increasing V .

Using this sharp change in the MA, we can realize a deterministic magnetization switching of the top LSMO layer without assistance from an external magnetic field. When V is changed from 200 mV to 15 mV, the easy axis along [110] at $V = 200$ mV becomes a hard axis at $V = 15$ mV, while the $[\bar{1}10]$ axis is always an easy axis. Thus, the magnetization initially pointed toward [110] at $V = 200$ mV is rotated toward $[\bar{1}10]$ when V is changed to 15 mV. Then, after V is returned to 200 mV from 15 mV, magnetization remains in that position ($[\bar{1}10]$). Meanwhile, when magnetization is initially pointed to $[\bar{1}10]$ at $V = 200$ mV, it remains fixed during the change in V .

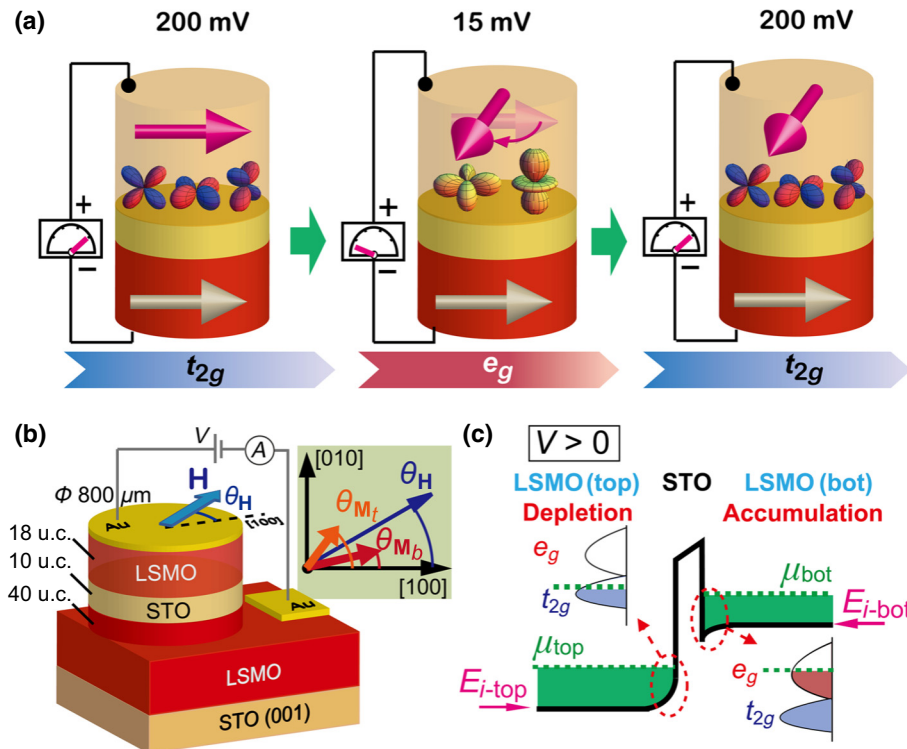


FIG. 1. (a) Deterministic and magnetic-field-free 90° -magnetization switching induced by slightly changing the bias voltage, V , applied to the MTJ. This phenomenon occurs with a change in the orbital symmetry from e_g to t_{2g} at the chemical potential (μ) of the top interface between LSMO (ferromagnetic layer) and STO (tunnel barrier). (b) Device structure and measurement configuration of the LSMO/STO/LSMO MTJ used in this study. (c) Band profile of the MTJ when V is positive; the green dotted lines represent the chemical potential levels (μ_{top} , μ_{bot}) in the top and bottom LSMO layers. There are carrier depletion and accumulation at the top and bottom LSMO/STO interfaces, respectively. Thus, when increasing V (> 0), the band character of the carriers at μ_{top} changes from e_g to t_{2g} symmetry at the top LSMO/STO interface (left inset).

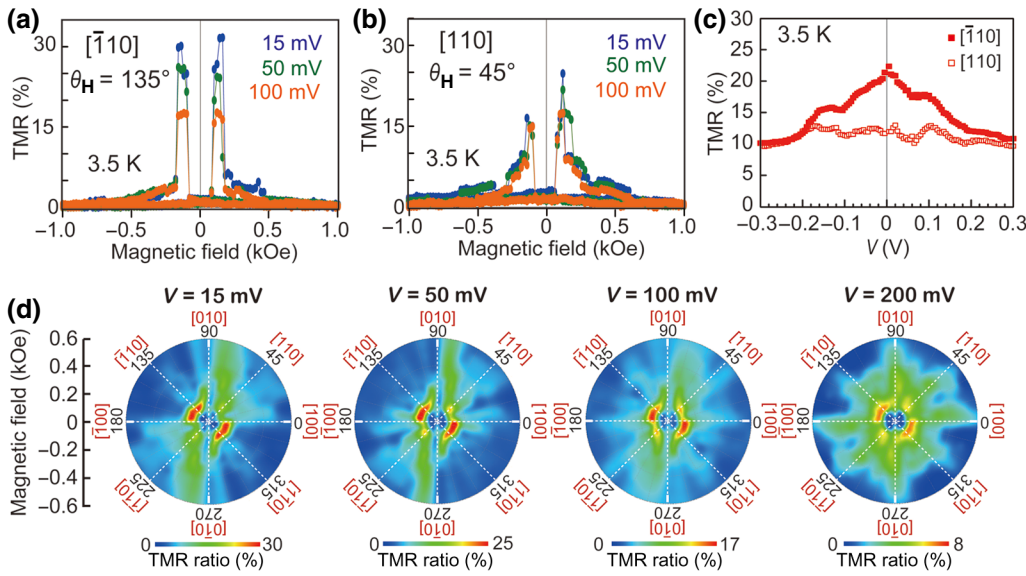


FIG. 2. (a),(b) \mathbf{H} dependence of TMR (major loops) measured at $V = 15, 50,$ and 100 mV, with \mathbf{H} applied in the film plane along $[\bar{1}10]$ (a) and $[110]$ (b). (c) Bias dependence of the TMR ratio, with \mathbf{H} applied along $[\bar{1}10]$ and $[110]$. (d) Polar color-mapping plots of the magnetic-field-direction dependence of TMR under a bias voltage of $V = 15, 50, 100,$ and 200 mV. All measurements are carried out at 3.5 K.

To verify this scenario, after applying $\mathbf{H} = 10$ kOe along $[110]$ or $[\bar{1}10]$ to align \mathbf{M}_t and \mathbf{M}_b with $V = 200$ mV, we measure the tunneling resistance, R , at zero magnetic field by varying V in the following sequence: 200 mV \rightarrow 15 mV \rightarrow 200 mV. In Figs. 3(a) and 3(b), the dotted horizontal lines, R_{P200} (R_{P15}) and R_{AP200} (R_{AP15}), express R values at $\mathbf{H} = 0$ when \mathbf{M}_t and \mathbf{M}_b are initialized in the parallel and antiparallel configurations at $V = 200$ mV (15 mV), respectively [23]. When \mathbf{M}_t and

\mathbf{M}_b are initialized along $[110]$ [Fig. 3(a)], one can see that the R value after the bias sequence does not return to R_{P200} , which indicates that \mathbf{M}_t is rotated during the bias sequence. We estimate the relative angle, $\Delta\theta$, of magnetization between the LSMO layers after the bias sequence, using the relation (see the Supplemental Material [23])

$$\cos \Delta\theta = \frac{2R_{P200}R_{AP200} - RR_{AP200} - RR_{P200}}{R(R_{AP200} - R_{P200})}. \quad (1)$$

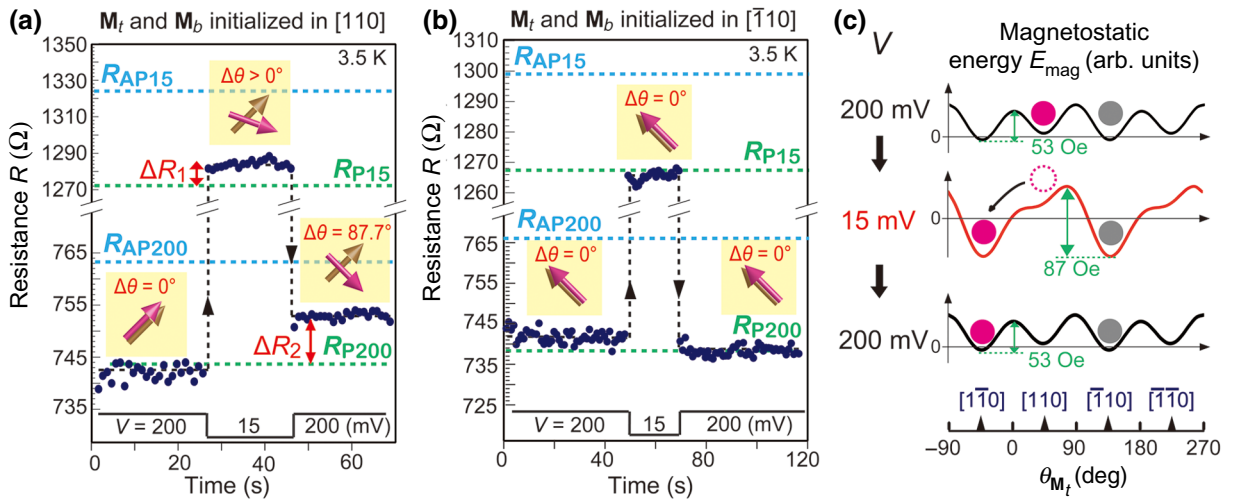


FIG. 3. (a),(b) Time evolution of the tunneling resistance, R , of the MTJ (dark blue dots) measured at zero magnetic field, with a bias sequence of $V = 200$ mV \rightarrow 15 mV \rightarrow 200 mV, after applying a strong $\mathbf{H} = 10$ kOe along $[110]$ (a) and $[\bar{1}10]$ (b) to align the magnetization vectors of the top and bottom LSMO, \mathbf{M}_t and \mathbf{M}_b . The pink and brown arrows in the yellow insets illustrate \mathbf{M}_t and \mathbf{M}_b in the film plane, respectively, which form an angle, $\Delta\theta$, determined using Eq. (1). In (a), R increases by ΔR_1 from R_{P15} and by ΔR_2 from R_{P200} after the bias sequence, due to the switching of \mathbf{M}_t . (c) Magnetostatic energy, E_{mag} , as a function of the magnetization direction, $\theta_{\mathbf{M}_t}$, of the top LSMO at $V = 200$ mV and 15 mV, calculated using the estimated anisotropy fields in Table I. The local minimum of E_{mag} at $[110]$ when $V = 200$ mV becomes unstable as V is decreased to 15 mV, while that at $[\bar{1}10]$ is always the minimum for all V . Thus, magnetization initially pointed toward $[110]$ (pink circle) at $V = 200$ mV rotates toward the $[\bar{1}10]$ direction at $V = 15$ mV, while that initially pointed toward $[110]$ (gray circle) at $V = 200$ mV stays fixed.

TABLE I. Parameters of the anisotropy fields obtained from the tunneling magnetoresistance data using the Stoner-Wohlfarth model: biaxial anisotropy field, $H_{4\langle 110 \rangle}$, along the $\langle 110 \rangle$ axes; uniaxial anisotropy field, $H_{2[110]}$, along the $[110]$ axis; uniaxial anisotropy field, $H_{2[100]}$, along the $[100]$ axis; the domain wall pinning energy, ϵ ; and the spin polarization, P , of the top and bottom LSMO layers.

Bias voltage (V)	Top LSMO layer				Bottom LSMO layer				P
	$H_{4\langle 110 \rangle}$ (Oe)	$H_{2[110]}$ (Oe)	$H_{2[100]}$ (Oe)	ϵ (Oe)	$H_{4\langle 110 \rangle}$ (Oe)	$H_{2[110]}$ (Oe)	$H_{2[100]}$ (Oe)	ϵ (Oe)	
0.015	250	-130	65	330	300	-50	20	170	0.13
0.05	420	-160	80	330	300	-50	20	170	0.11
0.1	480	-40	50	330	300	-50	20	170	0.08
0.2	350	-20	20	330	300	-50	20	170	0.04

The estimated $\Delta\theta$ value is 87.7° , which is in excellent agreement with the above expectation of 90° switching of magnetization. Furthermore, when \mathbf{M}_t and \mathbf{M}_b are initialized along $[\bar{1}10]$ [Fig. 3(b)], the MTJ consistently remains in the parallel magnetization configuration (i.e., $R = R_{P15}$ or R_{P200}), as expected. Magnetization switching occurs with an electric field of 0.05 V nm^{-1} ($=0.2 \text{ V}/3.9 \text{ nm}$), which is two orders of magnitude smaller than that needed for voltage-controlled MA ($\sim 1 \text{ V nm}^{-1}$) in previous reports [10–14]. The current density during this bias sequence is negligibly small: $1.3 \times 10^{-2} \text{ A cm}^{-2}$ (at $V = 200 \text{ mV}$) and $5.9 \times 10^{-4} \text{ A cm}^{-2}$ (at $V = 15 \text{ mV}$).

As shown below, this unusually large change in the MA is likely to be related to the change in the orbital at the chemical potential in the top LSMO layer (μ_{top}). This scenario of OCMS is strongly supported by the correlation between the changes in the MA fields and in the density of states (DOS) upon changing the magnetization direction. The derived MA fields of the LSMO layers, which we determine from the anisotropic TMR shown in Fig. 2(d) (see the Supplemental Material [23]), are summarized in Table I. When increasing V from 15 mV to 200 mV, the biaxial anisotropy field, $H_{4\langle 110 \rangle}$, increases by

40% (100 Oe), while the uniaxial anisotropy fields, $H_{2[110]}$ and $H_{2[100]}$ [24,25], rapidly decay and decrease by 85% (110 Oe) and 69% (45 Oe), respectively. This finding is consistent with the transition of the symmetry of the MA from two- to fourfold, as shown in Fig. 2(d). Using these MA fields, we calculate the magnetostatic energy, E_{mag} [Fig. 3(c)], which reproduces the result of magnetization switching shown in Figs. 3(a) and 3(b); the local minimum of E_{mag} at $[110]$, when $V = 200 \text{ mV}$ (filled pink circle), becomes unstable when decreasing V to 15 mV (dotted pink circle), while E_{mag} is always minimum at $[\bar{1}10]$ (filled gray circle). This result also confirms the validity of the derived MA fields.

The change in the DOS with magnetization direction is obtained by measuring dI/dV , with the application of a strong magnetic field of 1 T in various directions in the film plane, as shown in the color mapping of $\Delta(dI/dV)$ as a function of V and $\theta_{\mathbf{H}}$ ($=\theta_{\mathbf{M}}$ at $\mathbf{H} = 10 \text{ kOe}$) in Fig. 4(a) (see the Supplemental Material [23]). A clear change of about $\pm 1.5\%$ in dI/dV with twofold symmetry is induced by rotating \mathbf{H} . This result indicates that the DOS of the top and bottom LSMO layers change via the spin-orbit interaction when rotating the magnetization direction. The most

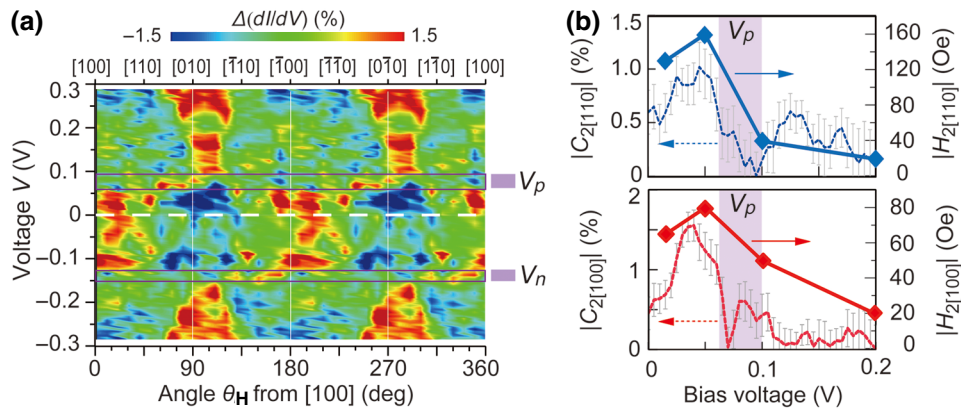


FIG. 4. (a) Color-mapping plot of $\Delta(dI/dV)$. The direction θ_{DOSmax} , along which dI/dV reaches its maximum, rotates by 90° at $V = V_p$ ($=0.6 \text{ V} - 0.95 \text{ V}$) and V_n ($[-0.15 \text{ V}] - [-0.13 \text{ V}]$) (purple bands). (b) Absolute values of the symmetry DOS components $C_{2[110]}$ and $C_{2[100]}$ are deduced from the magnetization-direction dependence of the DOS (dotted lines with error bars), and those of the anisotropy fields $H_{2[110]}$ and $H_{2[100]}$ are obtained from the TMR data at $V = 0.015, 0.05, 0.1, \text{ and } 0.2 \text{ V}$ (closed rhombuses), as functions of the bias voltage V . All measurements are carried out at 3.5 K.

important feature is that the direction, θ_{DOSmax} , of \mathbf{H} , the direction at which the DOS reaches its maximum, rotates by 90° when V is varied through $V_p = 0.06 \text{ V} - 0.095 \text{ V}$ and $V_n = (-0.15 \text{ V}) - (-0.13 \text{ V})$, which means that the orbital symmetry at E_F is changed with V [21]. We decompose the oscillation component of the $dI/dV - \theta_M$ curves into a fourfold component, $C_{4\langle 110 \rangle}$, along $\langle 110 \rangle$ and twofold components, $C_{2[100]}$ and $C_{2[110]}$, along $[100]$ and $[110]$, respectively. (For the derivation of the components $C_{4\langle 110 \rangle}$, $C_{2[100]}$, and $C_{2[110]}$, see the Supplemental Material [23].) As shown in Fig. 4(b), the absolute values of the twofold symmetry MA fields ($H_{2[110]}$ and $H_{2[100]}$) and those of the symmetry DOS components (i.e., $C_{2[110]}$ and $C_{2[100]}$) show very similar dependences on V . These findings suggest that the large MA change is induced by the change in the orbital symmetry at E_F . The scenario, however, needs to be solidified by more sophisticated calculations of the band structure and MA properties at the LSMO interfaces. A similar strong correlation between the MA and DOS symmetry has been reported for the ferromagnetic semiconductor (Ga,Mn)As [26]; this suggests the universality of this phenomenon for a wide variety of materials. Our result highlights the large potential of using band engineering techniques to manipulate magnetization.

In this work, as the bias voltage increases, the twofold MA disappears and is replaced with a fourfold one at the LSMO interface, which enables the one-way rotation of magnetization from $[110]$ to $[1\bar{1}0]$. For reversible control of the magnetization direction, the direction of the two- or fourfold easy magnetization axis should be changed with the bias voltage [e.g., in Fig. 3(c), the two-fold easy magnetization axis at $V = 15 \text{ mV}$ should be switched from $[1\bar{1}0]$ to $[110]$ at a different bias voltage]. Single-crystalline ferromagnetic quantum wells are promising candidates for reversible magnetization rotation, in which itinerant s,p electrons that are coupled with localized d electrons make resonant levels. Using the ferromagnetic quantum well, alternating reversal of the sign of the DOS symmetry, which may lead to an alternating change of the easy magnetization axis, is demonstrated when switching the on- and off-resonant states by changing the bias voltage [27].

Finally, we discuss the potential technological applicability of this OCMS method, which we have demonstrated only at the LSMO interface at low temperature (3.5 K) and in a large MTJ (800 μm in diameter) in this work. As shown in Fig. 3(c), the potential barrier between the $[110]$ and $[1\bar{1}0]$ magnetization directions at $V = 200 \text{ mV}$, which disappears at $V = 15 \text{ mV}$, is estimated to be 53 Oe, which corresponds to a MA constant, K_b , of 1.2 kJ m^{-3} . This large K_b value indicates that the two states of $[110]$ and $[1\bar{1}0]$ magnetization directions are thermally stable, even at room temperature. At the present temperature (3.5 K), even if we miniaturize the MTJ to as small as 21 nm in diameter, the thermal stability factor Δ is estimated to be 60.2. Here, $\Delta = K_b v / k_B T$, where v is the LSMO volume, and k_B

is the Boltzmann constant, and usually $\Delta > 60$ is required for a 10 year data retention time [28]. Furthermore, as the magnetization rotation is induced by the change in the MA energy, high-speed operation is, in principle, possible. Therefore, OCMS is technologically promising for state-of-the-art spin devices, if we can appropriately design the band structure of ferromagnetic materials.

ACKNOWLEDGMENTS

This work is partly supported by Grants-in-Aid for Scientific Research (Grants No. 18H03860 and No. 17H04922), the CREST Program (Grant No. JPMJCR1777) of the Japan Science and Technology Agency, and the Spintronics Research Network of Japan (Spin-RNJ).

-
- [1] J. Slonczewski, Current-driven excitation of magnetic multilayers, *J. Magn. Magn. Mater.* **159**, L1 (1996).
 - [2] L. Berger, Emission of spin waves by a magnetic multilayer traversed by a current, *Phys. Rev. B* **54**, 9353 (1996).
 - [3] J. Z. Sun and D. C. Ralph, Magnetoresistance and spin-transfer torque in magnetic tunnel junctions, *J. Magn. Magn. Mater.* **320**, 1227 (2008).
 - [4] I. M. Miron, K. Garello, G. Gaudin, P.-J. Zermatten, M. V. Costache, S. Auffret, S. Bandiera, B. Rodmacq, A. Schuhl, and P. Gambardella, Perpendicular switching of a single ferromagnetic layer induced by in-plane current injection, *Nature* **476**, 189 (2011).
 - [5] L. Liu, Chi-Feng Pai, Y. Li, H. W. Tseng, D. C. Ralph, and R. A. Buhrman, Spin-torque switching with the giant spin Hall effect of tantalum, *Science* **336**, 555 (2012).
 - [6] C.-G. Duan, J. P. Velev, R. F. Sabirianov, Z. Zhu, J. Chu, S. S. Jaswal, and E. Y. Tsybal, Surface Magnetoelectric Effect in Ferromagnetic Metal Films, *Phys. Rev. Lett.* **101**, 137201 (2008).
 - [7] K. Nakamura, K. Nakamura, R. Shimabukuro, Y. Fujiwara, T. Akiyama, T. Ito, and A. J. Freeman, Giant Modification of the Magnetocrystalline Anisotropy in Transition-Metal Monolayers by an External Electric Field, *Phys. Rev. Lett.* **102**, 187201 (2009).
 - [8] J. Stohr, H. C. Siegmann, A. Kashuba, and S. J. Gamble, Magnetization switching without charge or spin currents, *Appl. Phys. Lett.* **94**, 072504 (2009).
 - [9] N. N. Negulyaev, V. S. Stepanyuk, W. Hergert, and J. Kirschner, Electric Field as a Switching Tool for Magnetic States in Atomic-Scale Nanostructures, *Phys. Rev. Lett.* **106**, 037202 (2011).
 - [10] D. Chiba, M. Yamanouchi, F. Matsukura, and H. Ohno, Electrical manipulation of magnetization reversal in a ferromagnetic semiconductor, *Science* **301**, 943 (2003).
 - [11] W.-G. Wang, M. Li, S. Hageman, and C. L. Chien, Electric-field-assisted switching in magnetic tunnel junctions, *Nat. Mater.* **11**, 64 (2012).
 - [12] T. Maruyama, Y. Shiota, T. Nozaki, K. Ohta, N. Toda, M. Mizuguchi, A. A. Tulapurkar, T. Shinjo, M. Shiraishi, S. Mizukami, Y. Ando, and Y. Suzuki, Large voltage-induced

- magnetic anisotropy change in a few atomic layers of iron, *Nat. Nanotech.* **4**, 158 (2009).
- [13] Y. Shiota, T. Nozaki, F. Bonell, S. Murakami, T. Shinjo, and Y. Suzuki, Induction of coherent magnetization switching in a few atomic layers of FeCo using voltage pulses, *Nat. Mater.* **11**, 39 (2012).
- [14] S. Kanai, F. Matsukura, and H. Ohno, Electric-field-induced magnetization switching in CoFeB/MgO magnetic tunnel junctions, *Appl. Phys. Lett.* **108**, 192406 (2016).
- [15] J. T. Heron, J. L. Bosse, Q. He, Y. Gao, M. Trassin, L. Ye, J. D. Clarkson, C. Wang, J. Liu, S. Salahuddin, D. C. Ralph, D. G. Schlom, J. Iniguez, B. D. Huey, and R. Ramesh, Deterministic switching of ferromagnetism at room temperature using an electric field, *Nature* **516**, 370 (2014).
- [16] U. Bauer, L. Yao, A. J. Tan, P. Agrawal, S. Emori, H. L. Tuller, S. V. Dijken, and G. S. D. Beach, Magnetoionic control of interfacial magnetism, *Nat. Mater.* **14**, 174 (2015).
- [17] M. Tsujikawa, S. Haraguchi, T. Oda, Y. Miura, and M. Shirai, Giant magnetic tunneling effect in Fe/Al₂O₃/Fe junction. A comparative ab initio study on electric-field dependence of magnetic anisotropy in MgO/Fe/Pt and MgO/Fe/Au films, *J. Appl. Phys.* **109**, 07C107 (2011).
- [18] A. Asamitsu, Y. Moritomo, Y. Tomioka, T. Arima, and Y. Tokura, A structural phase transition induced by an external magnetic field, *Nature* **373**, 407 (1995).
- [19] J.-H. Park, E. Vescovo, H.-J. Kim, C. Kwon, R. Ramesh, and T. Venkatesan, Direct evidence for a half-metallic ferromagnet, *Nature* **392**, 794 (1998).
- [20] M. Bowen, A. Barthélémy, M. Bibes, E. Jacquet, J.-P. Contour, A. Fert, F. Ciccacci, L. Duò, and R. Bertacco, Spin-Polarized Tunneling Spectroscopy in Tunnel Junctions with Half-Metallic Electrodes, *Phys. Rev. Lett.* **95**, 137203 (2005).
- [21] L. D. Anh, N. Okamoto, M. Seki, H. Tabata, M. Tanaka, and S. Ohya, Hidden Peculiar Magnetic Anisotropy at the Interface in a Ferromagnetic Perovskite-Oxide Heterostructure, *Sci. Rep.* **7**, 8715 (2017).
- [22] J. D. Burton and E. Y. Tsybal, Tunneling anisotropic magnetoresistance in a magnetic tunnel junction with half-metallic electrodes, *Phys. Rev. B* **93**, 024419 (2016).
- [23] See Supplemental Material at <http://link.aps.org/supplemental/10.1103/PhysRevApplied.12.041001> for details on experimental and theoretical methods.
- [24] A. Vailionis, H. Boschker, W. Siemons, E. P. Houwman, D. H. A. Blank, G. Rijnders, and G. Koster, Misfit strain accommodation in epitaxial ABO₃ perovskites: Lattice rotations and lattice modulations, *Phys. Rev. B* **83**, 064101 (2011).
- [25] M. Mathews, F. Postma, J. Lodder, R. Jansen, G. Rijnders, and D. Blank, Step-induced uniaxial magnetic anisotropy of La_{0.67}Sr_{0.33}MnO₃ thin films, *Appl. Phys. Lett.* **87**, 242507 (2005).
- [26] H. Saito, S. Yuasa, and K. Ando, Origin of the Tunnel Anisotropic Magnetoresistance in Ga_{1-x}Mn_xAs/ZnSe/Ga_{1-x}Mn_xAs Magnetic Tunnel Junctions of II-VI/III-V Heterostructures, *Phys. Rev. Lett.* **95**, 086604 (2005).
- [27] I. Muneta, T. Kanaki, S. Ohya, and M. Tanaka, Artificial control of the bias-voltage dependence of tunnelling-anisotropic magnetoresistance using quantization in a single-crystal ferromagnet, *Nat. Commun.* **8**, 15387 (2017).
- [28] A. D. Kent and D. C. Worledge, A new spin on magnetic memories, *Nat. Nanotechnol.* **10**, 187 (2015).